

DEVELOPMENT AND VERIFICATION OF A MATERIAL MODEL FOR PREDICTION OF CONTAINMENT SAFETY OF EXHAUST TURBOCHARGERS

Dieter Memhard^{*}, Florence Andrieux^{*}, Dong-Zhi Sun^{*}, R. Häcker^{**}

^{*}Fraunhofer Institute for Mechanics of Materials IWM
Woehlerstrasse 11, 79108 Freiburg, Germany

^{**} Bundesanstalt für Materialforschung und –prüfung BAM
Unter den Eichen 87, 12205 Berlin, Germany

Abstract

For predicting the containment safety of turbochargers against failure of rotors at elevated temperatures and dynamic loading the complex deformation and damage behaviour of the respective materials has to be determined by appropriate experiments and on the other hand the temperature and strain rate dependency has to be described by a material model to simulate the component behaviour under these complex loading conditions. The investigations focus on the cast iron alloy EN-GJS-400 with nodular graphite. Its mechanical behaviour under uniaxial and multiaxial tension as well as under compression and shear loading has been investigated for a variety of loading rates and temperatures.

For the numerical modelling of the containment safety of turbochargers a material model has been developed with the capability to describe the specific deformation behaviour of casting materials, e.g. different properties under tension and compression, temperature and strain rate dependence. The deformation behaviour was described with a model for thermally activated flow and the damage behaviour with a Johnson-Cook type model and an extended failure model (bi-failure model) respectively.

The material model has been verified by numerical simulations of penetration tests under highly dynamic impact loading conditions. Also a containment test on a turbocharger was simulated.

Keywords:

Turbochargers, containment safety, highly dynamic loading, elevated temperatures, complex deformation, damage, failure, cast iron with nodular graphite, tension, compression, shear loading, different properties under tension and compression, temperature and strain rate dependency

Introduction

For modern diesel engines more and more bigger and faster spinning turbochargers are employed to enhance the power of the engines. As a consequence, the higher rotational energies of the turbine wheel and the compressor wheel respectively must be absorbed by the containment in case of bursting of the spinning wheels.

To prove the safety of the turbochargers containment tests are carried out at specific testing facilities. These tests are highly expensive and deliver only information for the specific turbocharger and testing condition. Thus, there is demand for appropriate numerical tools to reduce the development costs for turbochargers. Therefore the manufacturers are interested in material models to describe the deformation and failure behaviour of the containment under their specific loading conditions.

For the numerical modelling of the containment safety of turbochargers a material model has been developed with the capability to describe the specific deformation behaviour of casting materials, e.g. different properties under tension and compression as a function of stress triaxiality, temperature and strain rate dependence under large plastic deformations. The parameters for modelling the material behaviour of the cast iron alloy EN-GJS-400 have been determined for a variety of small scale specimen geometries with different triaxialities for a variety of strain rates and temperatures and then the model has been validated by tests under impact loading and a burst test respectively. The material model has been implemented as User material subroutine in the finite element code LS-DYNA

1. Characterization of the material behaviour

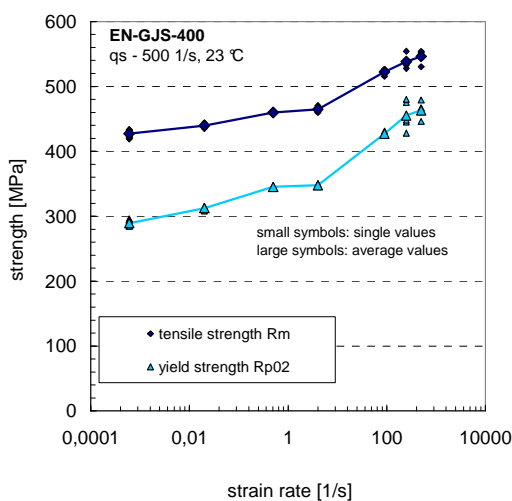
The cast iron alloy EN-GJS-400 with nodular graphite was in the focus of the investigations. A variety of tests on different specimens under compression, uniaxial and multiaxial tension as well as shear loading have been performed to characterize the deformation and failure behaviour.

1.1. Material characterization

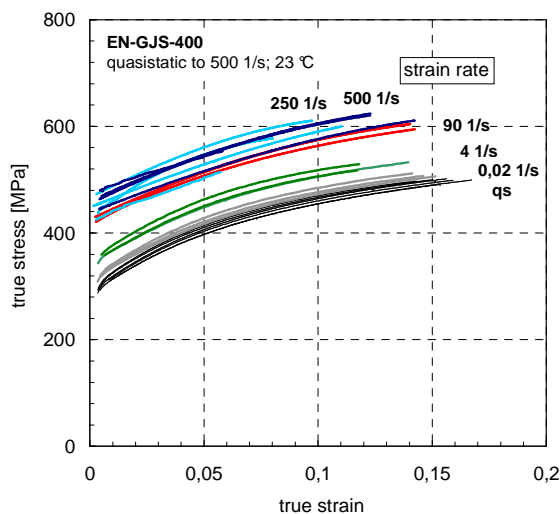
The casting material was delivered in plates with a thickness of 25 mm. The microstructural investigations of the alloy EN-GJS-400 show a ferritic matrix with nodular graphite and small fractions of pearlite.

1.2. Tension tests on smooth round bars

In [Figure 1](#) the yield strength $R_{p0,2}$, the tensile strength R_m and the flow curves are illustrated as a function of strain rate from 0,0006 1/s (quasi static) up to 500 1/s for 23 °C.



a)



b)

Figure 1: Casting material EN-GJS-400, a) strength values and b) flow curves as a function of strain rate from 0,0006 1/s to 500 1/s, 23 °C [1]

For high strain rates, e.g. 250 1/s, that are rather representative for the impact loading of the containment, strength values are decreasing with increasing temperature (Figure 2). Figure 2

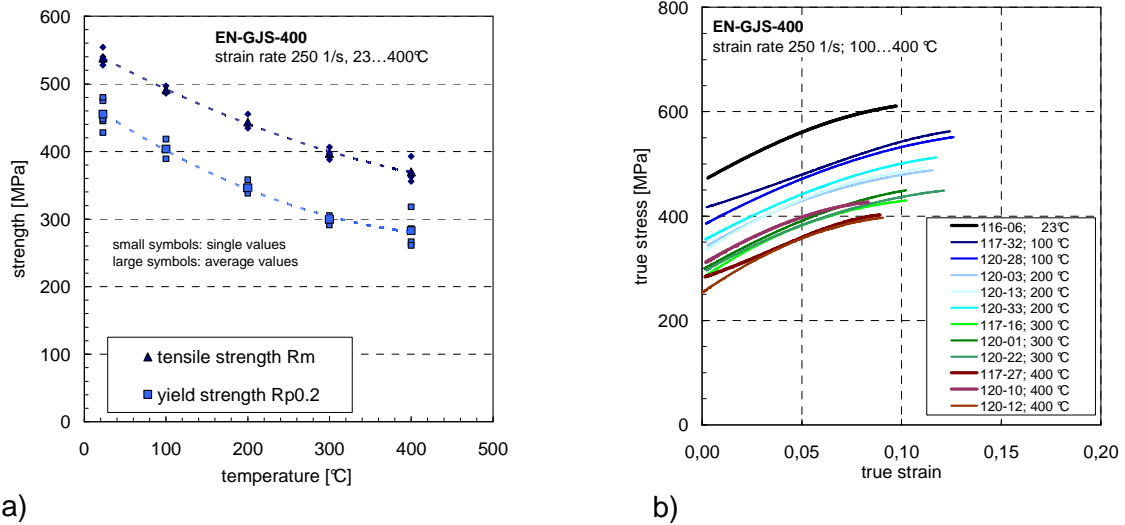


Figure 2: Casting material EN-GJS-400, a) strength and fracture strain values and b) flow curves as a function of temperature between 23 °C and 400 °C, s train rate 250 1/s [1]

1.3. Compression tests on cylindrical specimens

Compression tests on cylindrical specimens have been performed in the temperature range between 23 °C and 400 °C under quasi static conditions. Figure 3 shows the flow curves from tests at 23 °C, making clear that there were some surface cracks but no total failure of the entire specimen. For the failure curve the conservative assumption was made, that failure would occur as a consequence of these surface cracks.

1.4. Tension tests on notched specimens

Tests on notched tension specimens were carried out to deliver fracture strain values at higher triaxialities. As an example the curves in Figure 3 show a decrease of specimen elongation with decreasing notch radius ($R3 \rightarrow R1$) in comparison with the unnotched specimen.

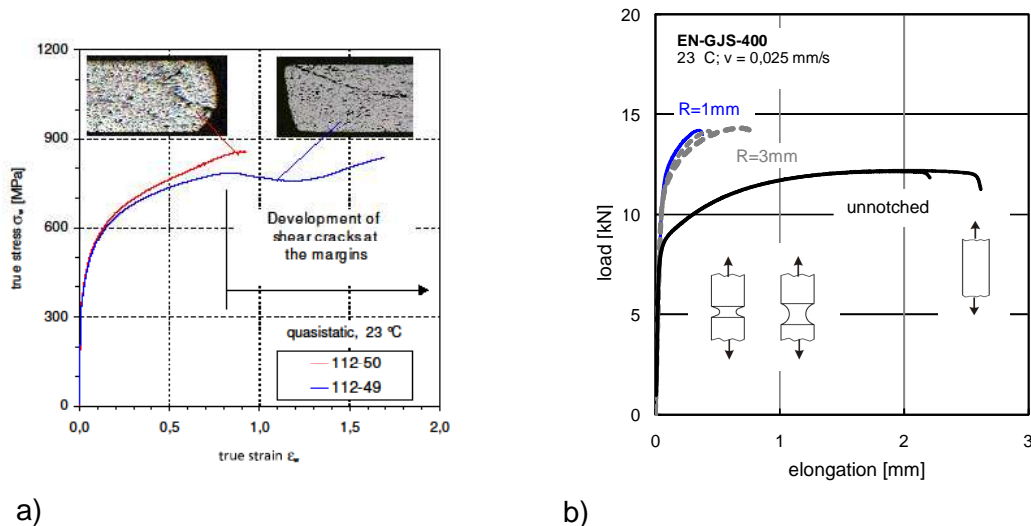


Figure 3: Casting material EN-GJS-400, a) flow curves from compression tests at 23 °C under quasi static conditions b) load-displacement records from tension tests on notched round bars [1]

1.5. Torsion tests on notched round bars

Since shear tension tests on notched tension bars failed to achieve shear dominated failure, torsion load was imposed on a notched round bar, relying on a proposal from Barsoum und Faleskog [2], who investigated notched pipes under torsion loading. Results are shown in chapter 4.1.1.

2. Analysis of the deformation and failure behaviour of the cast iron material and the consequences for numerical modelling

The microstructure of the cast iron material is characterized by a ferritic matrix with embedded nodular graphite particles that have an impact on the deformation and failure behaviour of the respective material. [Figure 4](#) shows the final stage of material behaviour in the tension (a) and the compression (2) test.

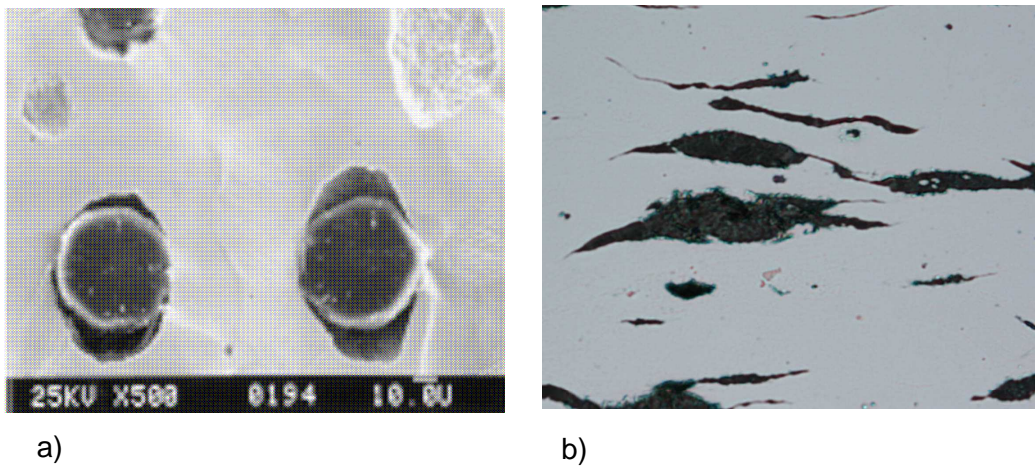


Figure 4: Deformation of the nodular graphite under tension and compression loading

- void decohesion from the base metal and void growth under tension [3],
- large deformation of the graphite particles under compression without decohesion

This cast iron behaves like a porous material under tension load whereas under compression it is almost incompressible.

3. Development of a material model for deformation and failure of cast iron with strain rate and temperature dependence

The constitutive model described below is intended for modelling the elastic-plastic behaviour of cast iron characterized by following macroscopic properties:

- different yield strengths in tension and compression with the yield stress under compression being then the yield stress under tension,
- different hardening behaviour under tension and compression ([Figure 5](#)),
- inelastic volume change in tension (dilatation) but no inelastic volume change in compression,
- decreasing ductility with increasing triaxiality, but at zero mean stress (obtained from a shear test) the fracture strain can be below the one obtained at significantly higher mean stress,
- strain-rate and temperature dependence of yield strength and failure strain,
- temperature dependent elastic modulus.

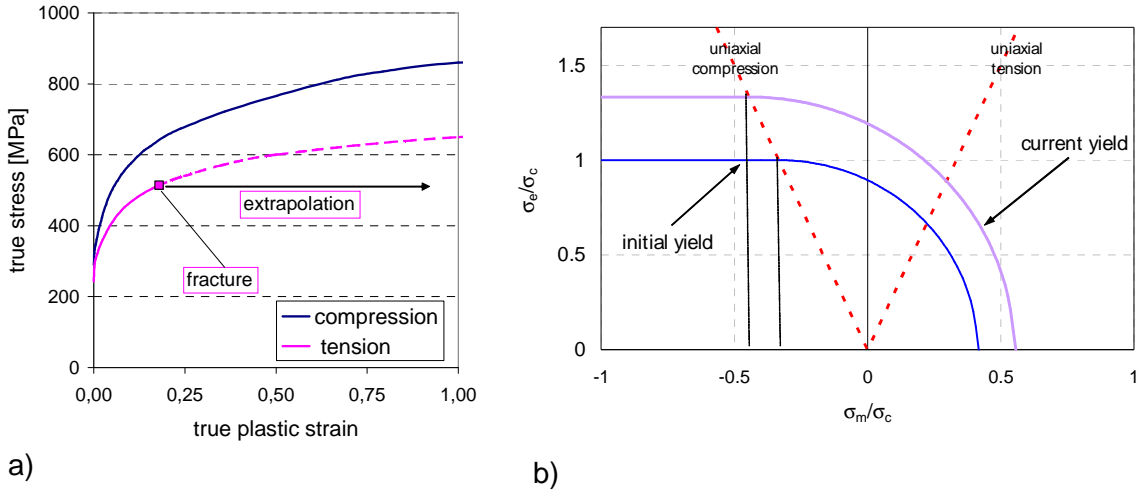


Figure 5: a) Flow behaviour of the cast iron material EN-GJS-400 under uniaxial stress and compression load
 b) Normalized yield surface of the cast iron material in the (σ_e, σ_m) -space at the beginning of yielding and after strain hardening

The asymmetric yield function Φ in the (σ_e, σ_m) -space is a half-ellipse in the region from the uniaxial compression to hydrostatic tension and the Mises straight line in the region to the hydrostatic compression to the uniaxial compression (Figure 5). σ_m denotes the mean stress and σ_e the von Mises stress. The triaxiality is defined as $T = \sigma_m / \sigma_e$.

$$\Phi = \tilde{\sigma} - \sigma_c \leq 0 \quad \tilde{\sigma}^2 = \begin{cases} \sigma_e^2 + \alpha^2 (\sigma_m + \frac{1}{3} \sigma_c)^2 & T \geq -\frac{1}{3} \\ \sigma_c^2 & T < -\frac{1}{3} \end{cases} \quad (1)$$

$$\text{with } \sigma_e = \sqrt{\frac{3}{2} \sigma'_{ij} \sigma'_{ij}}, \quad \sigma_m = \frac{1}{3} \sigma_{kk}; T = \sigma_m / \sigma_e$$

In (1) α is the parameter governing the shape of the half-ellipse centred at $-\sigma_c/3$. The asymmetry in the yield shape with respect to the mean stress accounts for different yield strength under uniaxial compression σ_c and uniaxial tension σ_t . The shape of the yield surface α is deduced from the initial yield stresses in compression and tension, σ_c^0 and σ_t^0 .

To describe the fracture behaviour a Johnson-Cook type fracture criterion was incorporated into the model, it means the strain at failure ϵ_f is given as a function of the stress triaxiality $T = \sigma_m / \sigma_e$, the equivalent plastic strain rate and the temperature. For the description of the failure behaviour three different types of failure curve have been investigated and are shown in Figure 6:

- Fracture strain independent of triaxiality T ($\epsilon_f = \text{const.}$), data from tension tests on smooth round bars,
- Fracture strain decreases monotonically with triaxiality T (Johnson-Cook), data from tests on specimens with different triaxiality (e.g. compression, uniaxial and multiaxial tension),
- Fracture strain with two regions of different failure mechanisms ($T < T_{\text{trans}}$ and $T > T_{\text{trans}}$) as well as a minimum for pure shear (bi-failure) [5, 6], data from tests on specimens with different triaxiality values (e.g. compression, shear as well as uniaxial and multiaxial tension).

Fracture occurs when the cumulative damage parameter D defined by (2) reaches the critical value of 1. Johnson-Cook proposed a linear damage accumulation. In this formulation a more general non linear damage accumulation is used:

$$\dot{D} = \frac{n}{\epsilon_f} D^{1-1/n} \dot{\epsilon}_p \quad (2)$$

In (2) ϵ_f^D denotes the equivalent plastic strain and the exponent n is a parameter.

The use of two distinct functions for failure strain is justified by the fact that different mechanisms lead to failure at low and high triaxialities. At high triaxialities failure is due to void growth and coalescence. The failure curve proposed by Johnson-Cook [4] for instance is relevant in this region. At low triaxialities shear failure is observed often at low failure strains.

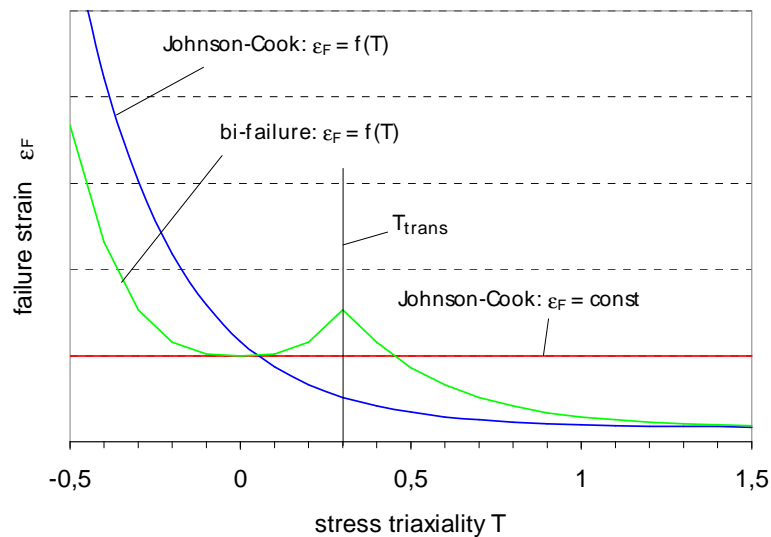


Figure 6: Schematic drawing for different types of failure curves with fracture strain as a function of triaxiality $T = \sigma_m / \sigma_e$

4. Finite element calculations of tests on small scale specimens for the determination of model parameters

4.1. Quasi-static und dynamic tension tests on smooth round bars

By numerical simulation of tension tests on smooth round bars at temperatures from 23 °C to 400 °C under quasi-static and dynamic loading up to strain rates of 500 s⁻¹ the parameters for the temperature and strain rate dependence of the flow behaviour have been determined. Under tension loading a plastic Poisson's ratio of $\nu_{pl} = 0.4$ materialises in the wake of plastic deformation giving evidence that the material is plastically compressible under tension loading.

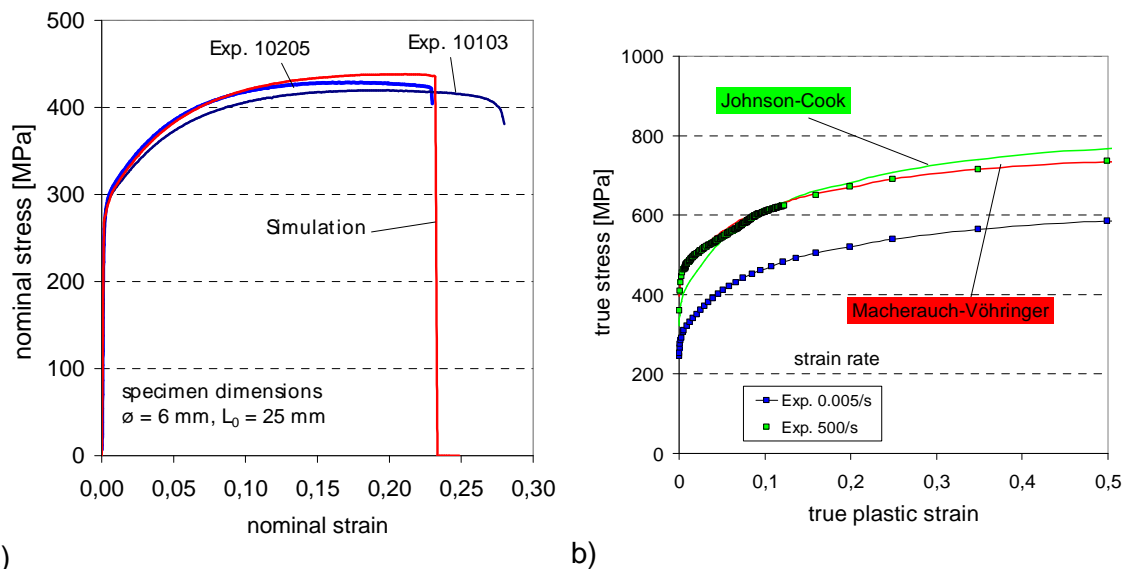


Figure 7: a) Upper and lower bound of engineering stress strain curves of the casting material EN-GJS-400 under quasi static loading and simulation of the lower bound test
 b) Calibration of the strain-rate dependency for quasi static loading up to 500 s⁻¹

Figure 7a shows the global response of the smooth tension bars under quasi static loading from experiment and numerical calculation. Two different models to describe the temperature and strain rate dependence of plastic flow and hardening have been investigated. Unlike the Johnson-Cook equation (4), the proposal from Macherauch and Vöhringer [7] proved to be a better approach for the flow behaviour of bcc metals. It relies on the micro mechanisms of thermally activated flow that proved to be a good approach for most ferritic steels. It separates the flow stress in a thermally activated part σ_a^* and a thermally inactive part σ_i (Eq. 3).

<p>temperature and strain rate dependence of flow stress after Macherauch-Vöhringer [7]</p>	$\sigma_C = \sigma_i + \sigma_a^*$ $= \Sigma_c(\epsilon_C) (1 - T^{*m}) + \sigma_a \left[1 - \left[\frac{kT}{\Delta G_0} \ln \frac{\dot{\epsilon}_a}{\dot{\epsilon}_c} \right]^{n_a} \right]^{m_a}$ <p>and</p> $T^* = \frac{T - T_{ref}}{T_{mel} - T_{ref}} \quad \text{for } T_{ref} < T < T_{mel}$ $= 0 \quad \text{for } T < T_{ref}$ $= 1 \quad \text{for } T > T_{mel}$	<p>(3)</p>
<p>flow stress after Johnson-Cook [4]</p>		<p>(4)</p>

Figure 7b illustrates that the model of Macherauch and Vöhringer is a better approach to describe the strain rate dependence of the cast iron.

4.1.1. Torsion tests on notched specimens

Figure 8 shows the load-displacement record from experiments and numerical calculations as well as a macrograph of the fracture surface, revealing a broad annular zone in the narrowest cross section with strong shear deformations. The final stage of failure is characterized by a void shaped fracture surface topography. Stress triaxiality calculated in the numerical model is approximately zero in the shear zone.

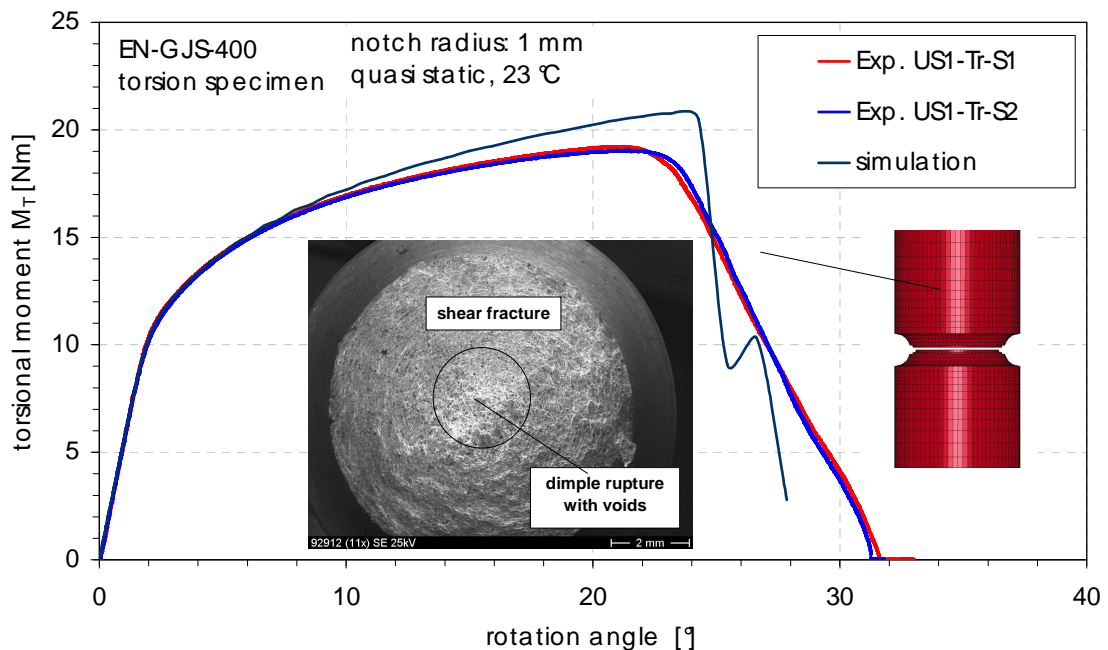


Figure 8: Failure of a torsion specimen of the cast iron material EN-GJS-400 under quasi static loading in the experiment and the numerical calculation

4.2. Determination of the failure curve from numerical analyses of the experiments

Figure 9 shows the different types of failure curves determined from the available experiments. A statistically relevant set of material does only exist for the smooth tension bars.

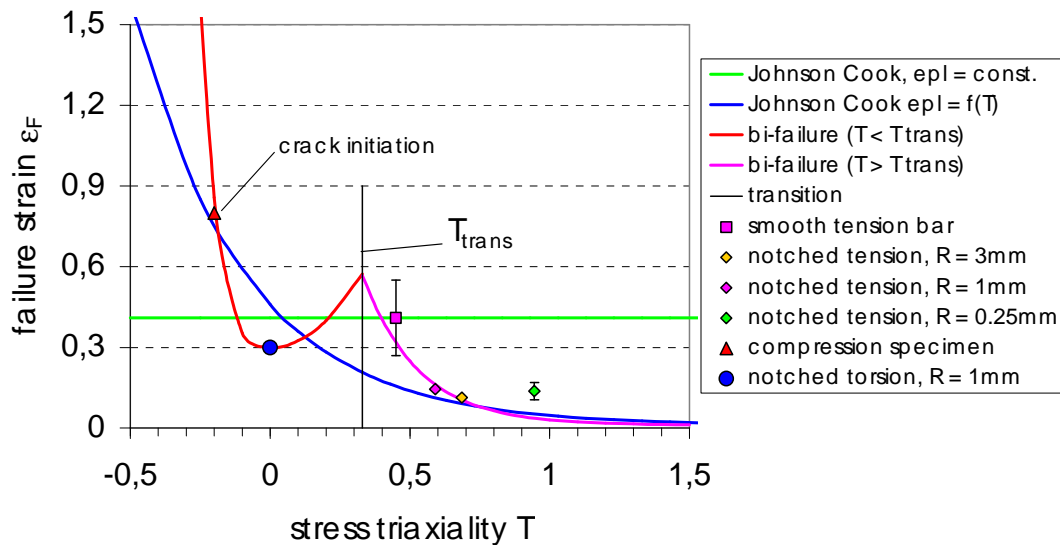


Figure 9: Failure curve options of the cast iron material EN-GJS-400 for numerical calculation of structures under complex loading; experimental data and approximated failure curve

4.3. Regularization

As the failure parameters are mesh size dependent and were determined above all on notched specimens, that necessarily had a fine mesh for accurate mapping of the notch geometry, a regularization of the failure strain has been performed for component simulations. A calibration function has been compiled for element sizes from 0.1 up to 16 mm by simulating the tests on flat tensile bars with the different element sizes.

5. Finite element simulations of experiments on bending specimens and assembly like structures for the validation of the material model

5.1. Notched bending specimens

As a first attempt for validation of the model quasi static experiments on notched bending specimens (Figure 10a) have been chosen. Figure 10b illustrates that the Johnson-Cook-failure curve ($JC=f(T)$) delivers a good approach for the global response of the specimen. A comparable result is achieved for the bi-failure-curve since failure is starting from the notch root, a high triaxiality region. The assumption of a constant failure strain ($JC = \text{const.}$) however, leads to an overestimation of the load bearing capacity of the specimen due to the neglect of the difference in fracture strain between tension and compression

5.2. Dynamic impact loading of plates

The containment safety of a turbocharger under the impact of fragments from a bursting rotor wheel was approached by an impact test with a high speed projectile hitting a plate. Figure 11 shows the back side of the plate that was penetrated by a cylindrical target with an initial velocity of 499 m/s [1] and the corresponding finite element model.

Calculations with all the three failure curves yielded failure velocities close to 500 m/s. The bi-failure model however yielded the best agreement with the impact tests, for the penetration velocity as well as for the appearance of the damage

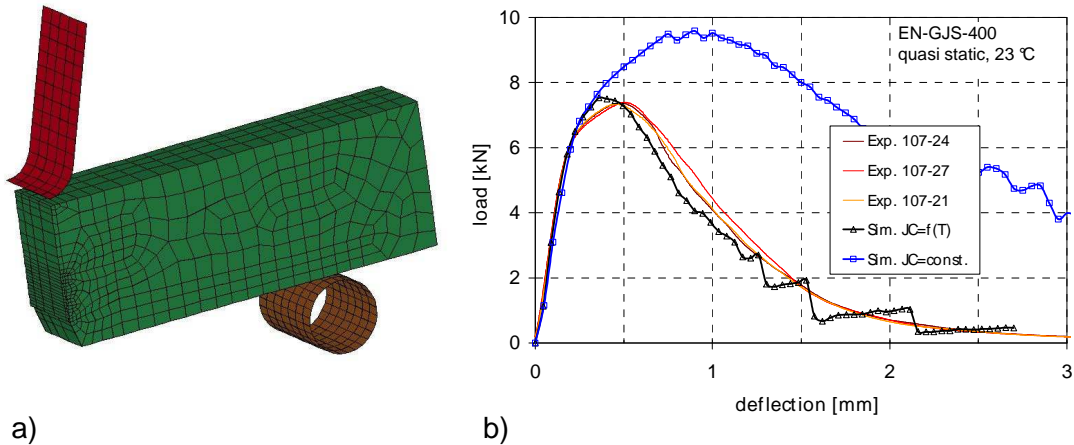


Figure 10: Numerical model of a notched bending specimen (a) and load-deflection curves (b) of the EN-GJS-400 material from experiments and numerical simulations

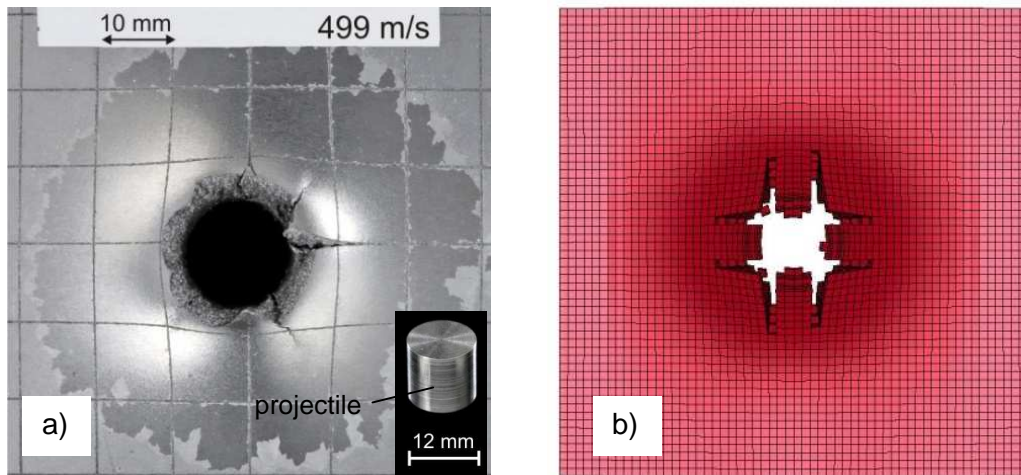


Figure 11: Damage of the plate after penetration of the projectile in the experiment (a) and the numerical simulation with the bi-failure-model (b)

Figure 12 illustrates the various phases of damage in the wake of the clash of the projectile on the plate and the following penetration of the plate. Damage and failure are initiated by the compression wave that is reflected and converted into a tension wave at the lower surface of the plate (1). As there is approximately biaxial loading in the contact zone with triaxialities > 0.5 failure in this region is triggered at low fracture strains (2). This failure zone spreads out over the whole thickness of the plate up to the lower surface of the projectile (3)-(4). The final phase of failure is dominated by the penetration of the projectile by shearing (5)-(6).

5.3. Simulation of a containment test of a fast spinning rotor

As an industrial application of the experimental and numerical investigations the simulation of a containment test [48] was carried out. For preparation of the test sample three notches were cut into the compressor wheel spaced 120 degrees apart. The compressor wheel would then burst during operation at the weakened sections due to high local stresses caused by the centrifugal forces.

Figure 13

Figure 13

Figure 13 shows the results for the insert piece. Cracks can be observed in regions of plastic strains greater than 35-40%.

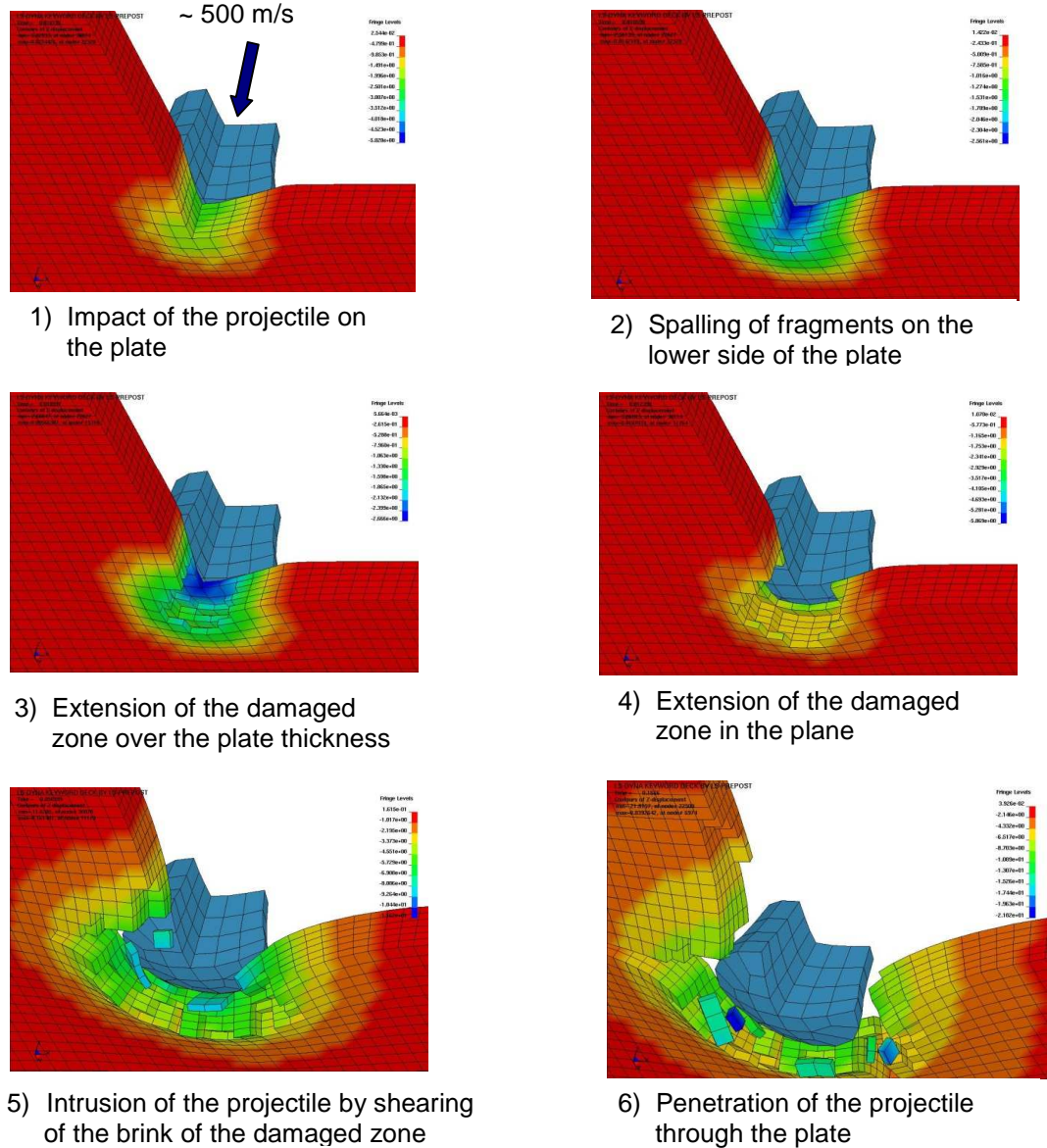


Figure 12: EN-GJS-400, penetration test, ~500 m/s, 23 °C, phases of damage and failure in the contact zone; simulation with the Johnson-Cook-model, $JC=f(T)$

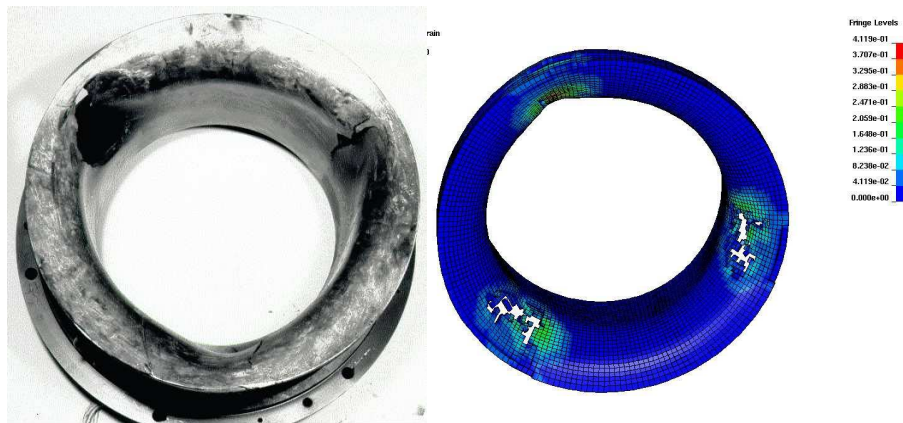


Figure 13: Insert piece of the compressor housing of cast iron EN-GJS-400 after the impact of the rotor segment, left the damage appearance (a) and right the corresponding numerical model with a plastic strain plot (b)

6. Summary

In this research project the ductile cast iron alloy EN-GJS-400 with nodular graphite was investigated. Its mechanical behaviour under uniaxial and multiaxial tension as well as under compression and shear loading has been examined for a variety of loading rates and temperatures. Since the investigations only concerned the containment but not the rotor of the turbocharger the loading of the whole device was approached by the impact of a plate by a projectile made of the same material.

A new material model was developed to model the special deformation and fracture behaviour of ductile cast iron alloys. The material parameters for the model have been determined by numerical modelling of small scale tests under different loading conditions. The material model has first been applied to numerical simulations of tests on notched specimens under bending load, then to the simulation of penetration tests under highly dynamic impact loading conditions and last to the containment test of a turbocharger. The loading conditions in the dynamic tests are comparable to the impact of a broken turbine blade on the containment of a turbocharger. The main purpose of these tests hence was to prove the prediction capability of the material model.

The calculated results agreed quite well with the experimental data. The model has been implemented in a commercial finite element code with explicit integration. In the actual version of the user subroutine the application is limited to solid elements.

7. Literatur

- [1] R. Häcker, E. Knothe, P. Wossidlo: Experimentelle Untersuchungen für die Anwendung von Materialmodellen zur numerische Auslegung des Containments von Abgasturbo ladern, Proceedings der Tagung Werkstoffprüfung, Dezember 2010 in Neu-Ulm, Hrsg. M. Pohl, S. 317-322.
- [2] J. Barsoum, J. Faleskog, Rupture mechanisms in combined tension and shear--Experiments, International Journal of Solids and Structures, 44, 2007, 5481-5498.
- [3] Dong, M.J., Prioul, C., François, D., Metallurgical and Material Transactions A 28A, 2245-2254, 1997.
- [4] G.R. Johnson and W.H. Cook, Fracture characteristics of three metals subjected to various strains, strain rates, temperatures and pressures, Engineering Fracture Mechanics, 21, No.1, (1985) 31-48.
- [5] Wierzbickie, T., Bao, Y., Lee, Y.-W., Bai, Y., Calibration and evaluation of seven fracture models, Int. Journal of Mechanical Sciences, 47 (2005), 719-743.
- [6] F. Andrieux, D.-Z. Sun, Damage modelling for simulation of process chain from forming to crash, Int. J. Mat. Res. 2010, 101, 8.
- [7] E. Macherauch, O. Vöhringer, Das Verhalten metallischer Werkstoffe unter mechanischer Beanspruchung, Z. für Werkstofftechnik, 9, 1978, 370-391.
- [8] T. Winter, A. Huß, H. Beck, Simulation of Containment-Tests of fast-spinning rotors by explicit FEM, 22nd CAD-FEM Users' Meeting, Nov. 2004.